2H/H and 18O/16O Non-Equilibrium Fractionation Factors for Ocean Evaporation in the North-West Atlantic Region

Daniele Zannoni[1], Hans Christian Steen-Larsen[2], Andrew J. Peters[3], Sonja Wahl[4], Harald Sodemann[2], and Árny Erla Sveinbjörnsdóttir[5]

[1]Geophysical Institute, University of Bergen and Bjerknes Centre for Climate Research
[2]University of Bergen
[3]Bermuda Institute of Ocean Sciences
[4]Geophysical Institute, University of Bergen, and Bjerknes Centre for Climate Research
[5]University of Iceland

November 23, 2022

Abstract

Isotopic evaporation models, such as the Craig-Gordon model, rely on the description of non-equilibrium fractionation factors that are, in general, poorly constrained. To date, only a few gradient-diffusion type measurements have been performed in ocean settings to test the validity of the commonly used non-equilibrium fractionation factor parametrizations for ocean evaporation. In this work we present six months of water vapor isotopic observations collected from a meteorological tower located in the northwest Atlantic Ocean (Bermuda) with the objective of estimating the best non-equilibrium fractionation factors (k, Gradient-diffusion measurements are sensitive enough to resolve non-equilibrium fractionation factors during evaporation and provide mean values of k18= 5.2±0.6 furthermore evaluate the relationship between k and 10-m wind speed over the ocean. Such relationship is expected from current evaporation theory and from laboratory experiments made in the 1970s, but observational evidence is lacking. We show that (i) sensitivity of k to wind speed is small, in the order of -0.16 to 0.20 empirical evidence for the presence of a discontinuity between smooth and rough wind speed regime during isotopic fractionation, as proposed in earlier studies. Instead, k18 monotonically decreases within our observed wind speed range [0 – 10 m/s]. Implications for using such k values in modelling ocean vapor d-excess are briefly discussed.

$^{2}H/H$ and $^{18}O/^{16}O$ Non-Equilibrium Fractionation Factors for Ocean Evaporation in the North-West Atlantic Region

D. Zannoni[1], H. C. Steen-Larsen[1], A. J. Peters[2], S. Wahl[1], H. Sodemann[1] and A. E. Sveinbjörnsdóttir[3]

[1]Geophysical Institute, University of Bergen and Bjerknes Centre for Climate Research, 5007, Bergen, NORWAY.
[2]Bermuda Institute of Ocean Sciences, St. George's GE01, BERMUDA.
[3]Institute of Earth Sciences, University of Iceland, Reykjavik, ICELAND.

Corresponding author: Daniele Zannoni (daniele.zannoni@uib.no)

Key Points:

- Distributions of main water isotopologues' non-equilibrium fractionation factors for evaporation in the North Atlantic Ocean are proposed.
- Significant correlation observed between non-equilibrium fractionation factors and 10-m wind speed.
- Observed non-equilibrium fractionation factors agree only in part with the established parametrization based on wind speed.
- No evidence of discontinuity in smooth and rough regimes for isotopic fractionation during ocean evaporation.

Abstract

Isotopic evaporation models, such as the Craig-Gordon model, rely on the description of non-equilibrium fractionation factors that are, in general, poorly constrained. To date, only a few gradient-diffusion type measurements have been performed in ocean settings to test the validity of the commonly used non-equilibrium fractionation factor parametrizations for ocean evaporation. In this work we present six months of water vapor isotopic observations collected from a meteorological tower located in the northwest Atlantic Ocean (Bermuda) with the objective of estimating the best non-equilibrium fractionation factors (*k, ‰*) for ocean evaporation and their dependency on wind speed. Gradient-diffusion measurements are sensitive enough to resolve non-equilibrium fractionation factors during evaporation and provide mean values of k_{18}= 5.2±0.6 ‰ and k_2= 4.3±3.4 ‰. In this study, we furthermore evaluate the relationship between *k* and 10-m wind speed over the ocean. Such relationship is expected from current evaporation theory and from laboratory experiments made in the 1970s, but observational evidence is lacking. We show that (i) sensitivity of *k* to wind speed is small, in the order of -0.16 to 0.20 ‰ $m^{-1}s$ for k_{18}, and (ii) there is no empirical evidence for the presence of a discontinuity between smooth and rough wind speed regime during isotopic fractionation, as proposed in earlier studies. Instead, k_{18} monotonically decreases within our observed wind speed range [0 – 10 m s^{-1}]. Implications for using such *k* values in modelling ocean vapor d-excess are briefly discussed.

Plain Language Summary

The theory behind non-equilibrium isotopic fractionation during ocean evaporation was formulated more than 50 years ago. However, still today there is little agreement on which are the best non-equilibrium fractionation factors to use in evaporation models. Currently, non-equilibrium fractionation factors are calculated following a parametrization based on wind speed experiments performed in the 1970s. This wind effect, which modulates the weight of molecular and turbulent transport of water vapor during evaporation has never been directly observed over the ocean. This study reports non-equilibrium fractionation factors for ocean evaporation estimated directly from flux measurements in an oceanic condition and explores their relationship with wind speed. Since having accurate fractionation factors is fundamental when modelling the Earth's water cycle with stable isotopes, the results of this study can help improving performances of General Circulation Models when describing ocean evaporation.

1 Introduction

Stable isotopes of hydrogen and oxygen in water have been used successfully for more than 50 years to study processes of the Earth's water cycle. Specifically, using water stable isotopes enables the atmospheric processes of the water cycle to be studied on time scales spanning mesoscale to glacial-interglacial time scales (Galewsky et al., 2016; Held & Soden, 2000). Modulation of the water vapor isotopic composition, hereafter in delta notation, is linked to several physical processes occurring in the atmosphere and is considered a proxy for the atmospheric water vapor thermodynamic state. For instance, isotope ratios of $^{18}O/^{16}O$ ($\delta^{18}O$) and $^{2}H/H$ (δD) in precipitation are largely controlled by upstream cloud formation during moisture transport and isotopic equilibrium effect during phase changes (Craig, 1961; Dansgaard, 1964; Rozanski et al., 1993). On the other hand, the deviation from the linear relationship between $\delta^{18}O$ and δD (i.e., d-excess=$\delta D-8*\delta^{18}O$) in precipitation is controlled by one-directional non-equilibrium effects linked to evaporative conditions of moisture source areas (Craig & Gordon,

1965; Merlivat & Jouzel, 1979; S. Pfahl & Sodemann, 2014), by moisture recycling above the continents as well as by sub-cloud droplet evaporation (Risi et al., 2013; Stewart, 1975) and cloud microphysics (Ciais & Jouzel, 1994).

1.1 Magnitude and control of non-equilibrium fractionation during ocean evaporation: objectives of the study

While isotopic fractionation effects during water phase changes in equilibrium conditions (above 0°C) are well understood, the non-equilibrium fractionation effects are still poorly constrained. During evaporation, a non-equilibrium process, the relative weight of molecular and turbulent diffusion controls the magnitude of non-equilibrium fractionation. While the values 0.9757 and 0.9727 are in general considered representative for $HD^{16}O/H_2{}^{16}O$ and $H_2{}^{18}O/H_2{}^{16}O$ molecular diffusivity in air (Merlivat, 1978), their weights during natural evaporation were estimated to be only ~1/4 of a pure molecular diffusion controlled process (Horita et al., 2008). To this end, a largely adopted parametrization of non-equilibrium fractionation factors involves wind speed as the only independent variable (Merlivat & Coantic, 1975). However, several recent studies have questioned the assumed role of sea surface temperature (SST) and wind speed on the controls of non-equilibrium fractionation based on water vapor d-excess observations (Bonne et al., 2019; Steen-Larsen et al., 2014; Steen-Larsen et al., 2015; Uemura et al., 2008). Other studies argued that d-excess may not be influenced solely by ocean surface evaporative conditions, namely relative humidity (RH) and SST, but also by the Marine Boundary Layer (MBL) height and by the moisture input from the free troposphere (Benetti et al., 2018; Galewsky et al., 2022). Consequently, it can be concluded that a large uncertainty exists on the magnitude of non-equilibrium fractionation during evaporation in real-environmental conditions and, still, no agreement exists on the controls of non-equilibrium fractionation by SST and wind speed (e.g. Gonfiantini et al., 2020). This lack of consensus drives the following questions: which non-equilibrium fractionation factors are the most accurate to use during the evaporation process in the marine boundary layer? Is there empirical evidence for a dependency between non-equilibrium effects and wind speed in the oceanic environment? If a relationship between wind speed and non-equilibrium fractionation exists, is it captured by established parametrization based on wind tunnel experiments? And finally, what is the impact of MBL structure, ocean isotopic composition and SST variability on the estimation of evaporation flux composition during natural evaporation over the ocean? These research questions will be addressed in this study by:

1. Estimating the best non-equilibrium fractionation factors for $\delta^{18}O$ and δD that can explain the observed isotopic composition of evaporation flux from the ocean surface.
2. Test the validity of theoretical parametrization of the wind speed effect on non-equilibrium fractionation with observations of the isotopic composition of evaporation flux over the ocean.
3. Test the sensitivity of observed non-equilibrium fractionation factors against ocean isotopic composition and SST variability.

Furthermore, we discuss the implications for using the estimated non-equilibrium fractionation factors when modelling ocean vapor d-excess and how the height of MBL can explain a significant portion of the water vapor d-excess variability in the study area.

1.2 The problem of evaporation flux representativity in the isotopic composition of near-surface water vapor

In general, links between ocean conditions, non-equilibrium fractionation and d-excess are based on the assumption that observations of the d-excess signal in atmospheric water vapor are representative of local evaporation in steady state. This assumption, however, is no longer valid when measurements are performed in low evaporation areas or for periods when other prevailing water vapor exchange processes, such as advection, occur in the atmosphere. Therefore, the wind speed effect could be smoothed out in vapor d-excess signal by other processes. Observations of water vapor isotopic composition at a single height level then might not be representative of the evaporation flux. Instead, profile observations of water vapor isotopic composition in ocean settings are particularly beneficial to estimate the isotopic composition of the evaporation flux. Many profile measurements are available in continental settings from atmospheric research and flux towers (e.g. Griffis et al., 2016) but such type of measurements is scarce for the ocean. Most of the available profile observations over the ocean were acquired for short time frames with low-temporal resolution techniques in the past (Gat et al., 2003; Craig & Gordon, 1965). More recently, two-heights profiles were acquired during cruises but introducing some additional uncertainties due to the use of different instruments for isotopic analysis at each height, ship movement, ship exhaust and ocean spray contribution to the vapor composition (Thurnherr et al., 2020). In this study we analyze six months (20th June to 30th December 2013) of continuous observations of water vapor isotopic composition sampled at two heights from a meteorological tower located in the northwest Atlantic region (Bermuda, Figure 1).

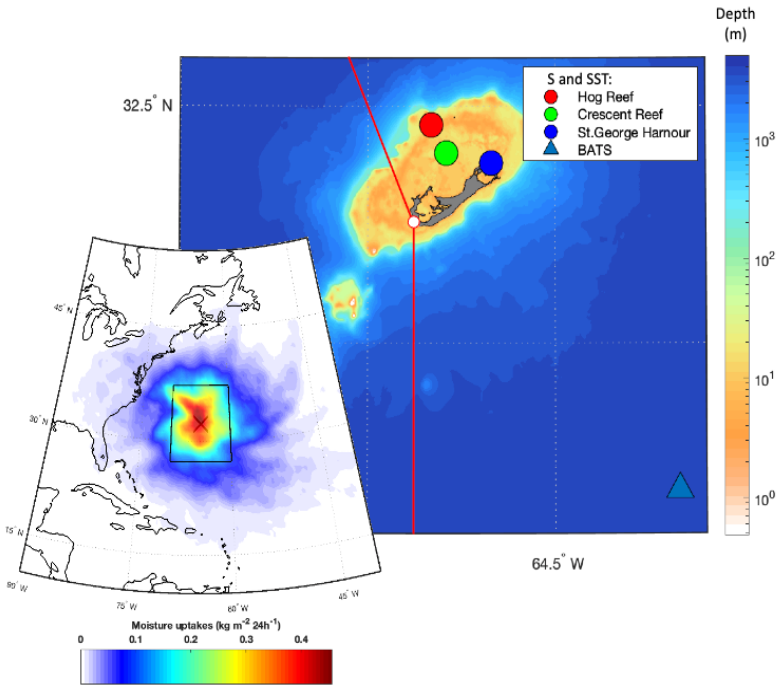

Figure 1: Study site of water vapor isotopic composition in Bermuda. Bermuda Island shape in dark grey and water depth as color scale (Hijmans, 2015; NOAA, 2019): position of Tudor Hill Marine Atmospheric Observatory (white dot) and wind sector to discriminate local transpired water vapor (red lines). Colored circles and triangle are the sampling locations of available salinity and SST time series around the study area. The large-scale map on the left

shows the location of Bermuda (cross) in the northwest Atlantic Ocean and the main water vapor sources during the study period. The highlighted sector includes 45% of accounted water vapor uptakes.

Due to its position and climatic conditions, the island of Bermuda is an ideal study site for evaporation-related processes and their control on the d-excess signal because ocean evaporation is the dominant source of the marine boundary layer vapor and there is low influence of continental water vapor. Given that Bermuda is located in part of the source region for the precipitation which is deposited in Greenland, this study is also relevant for ice core science (Faber et al., 2020; Johnsen et al., 1989; H. Sodemann et al., 2008). Specifically, it poses new questions about the information deduced from climate proxies in paleoclimate archives (e.g. Jouzel et al., 2007; Steen-Larsen et al., 2011, Markle et al., 2018). Therefore, the sensitivity of non-equilibrium fractionation factors to ocean composition and to SST variability and the impact on the d-excess sensitivity to evaporative condition over the ocean are also discussed.

2 Materials and Methods

2.1 Study site

The study site is located in the south-western part of the Bermuda Main Island, at the Tudor Hill Marine Atmospheric Observatory (THMAO) tower of Bermuda Institute of Ocean Sciences (32.26° N 64.88° W). The THMAO tower faces the coast (distance ~30m) and is 20.5 m high. Considering the altitude of the tower base (~29 m AMSL), the top of the tower faces the ocean at a height of ~50 m AMSL. The climatic conditions at Bermuda Island are characterized by humid subtropical climate, strongly affected by the Gulf Stream. The study area is situated in the so-called Bermuda-Azores High, a large subtropical center of high atmospheric pressure. The high-pressure system is strong and centered near the Bermuda Islands during the summer and related to the intensity of the Icelandic Low. Ocean evaporation around Bermuda Island is strong due to its location in Gulf Stream area and by the influence of unsaturated air transported off the American Continent, especially during the winter. ERA5 reanalysis data (Hersbach et al., 2020) shows that the evaporation flux (E) in the study area exceeds the precipitation flux (P), as expected (P-E = -1.34 mm day^{-1}). WaterSip moisture source diagnostic (Sodemann & Läderach, 2021) for the Jun-Dec 2013 calculated with 1˚x1˚ 6h time step resolution ERA-Interim reanalysis (Dee et al., 2011) revealed that 45% of lower tropospheric moisture originated in a 10˚x10˚ area around the study site (inset map in Figure 1).

2.2 Meteorological and ocean observations

Air temperature, relative humidity (T, RH, Campbell Scientific EE181-L125-PT), wind speed and wind direction (WS, WD, R.M. Young CAT NO. 05103) were measured at the top inlet (50 m AMSL) of THMAO. The wind speed measured at 50 m ASL was corrected to 10 m AMSL assuming a log-law wind profile and a roughness length of 0.2 mm (Stull, 1997). Sea Level Pressure (SLP) and precipitation (P) were measured ~20 km northeast at the L. F. Wade International Airport (TXKF) by the Bermuda Weather Service. Boundary Layer Height (BLH) data was taken from ERA5 global reanalysis at 0.25°x0.25° and 1-hour temporal resolution. BLH gridded data was linearly interpolated at the study site location.

2.3 SST and Ocean water isotopic composition

Salinity and SST observations are available from buoys inside the reef at 3h time resolution (Hog Reef and Crescent Reef), at St.George Harbor at daily resolution and outside the reef at monthly

resolution for the Bermuda Atlantic Time-series Study (BIOS, 2021). Salinity and SST measurement locations are reported in Figure 1. To minimize potential bias due to local SST variations we chose the averaged Operational Sea Surface Temperature and Sea Ice Analysis (OSTIA, UK MET OFFICE, 2005) data as representative for SST of the study site. High correlation is observed between average SST measured inside the reef and OSTIA product (R Pearson> 0.96) but better agreement, in terms of maximum absolute difference, was observed between BATS and OSTIA data (1.08 ˚C) than for Crescent reef and OSTIA data (2.55 ºC).

No measurements of ocean water isotopic composition near the study site are available for the period of interest, but the temporal variability of the ocean isotopic composition in the study area is assumed to be very low. Several sources have been evaluated for estimating the most representative composition of ocean water around the study site: gridded dataset (LeGrande & Schmidt, 2006), North Atlantic cruises published data (Benetti et al., 2014, 2017) as well as from samples collected at the BATS site two years before this campaign (BIOS, 2021). The average isotopic composition of the ocean in this study is assumed to be $\delta^{18}O_L$ = 1.09‰ and δD_L = 7.25‰, which is the average of the salinity to isotope conversion (Benetti et al., 2017) from gridded dataset and BIOS data. Full details on ocean water isotopic composition are reported in Supporting Info, Text S1.

2.4 Water vapor isotopic composition and humidity observations

Ambient air was sampled at THMAO tower at two different heights: 2.5 m and at 50 m AMSL. Ambient air was continuously pumped from the two inlets to a manifold located at the tower base that was connected to a Picarro L2120-i isotopic water vapor Cavity Ring-Down Spectroscopy (CRDS) analyzer. Quick air transport was ensured through heated copper tubing using a 10 L min^{-1} sampling pump. The sampling line was switched between the two inlets every 15 minutes and when one inlet was connected to the analyzer, the other inlet was flushed by a secondary 5 l min^{-1} pump. This configuration ensured a continuous circulation of air inside the tubing system, thus minimizing the lag and memory effect for the two inlets. The CRDS analyzer recorded humidity and water isotopic composition at ~0.56 Hz frequency. To reduce the memory effect due to the switching between top and bottom inlet, the first 10 minutes of data after valve switching was removed and the last 5 minutes was averaged. In this way, the 5 minutes average is assumed to be representative of the isotopic composition during measurement for each level. The inlet can be approximated to a first-order low pass filter with transfer function $H=1/(\tau+1)$, where τ is the time the system's response need to reach 63% of the final value for a step change from zero initial condition ($\tau(\delta^{18}O)$ = 212 s, $\tau(\delta D)$ = 310s). We estimated that the magnitude of signal attenuation is only -1.9 dB for $\delta^{18}O$ and -3.4 dB for δD and the phase difference between $\delta^{18}O$ and δD signal is <9˚ with an averaging window of 0.5 hours. Therefore, the error introduced by signal attenuation and phase difference between $\delta^{18}O$ and δD signal in the sensing system is not significant at the time resolution used in this study.

The isotope readings of the water vapor analyzer were calibrated on the VSMOW-SLAP scale (IAEA, 2009) using several laboratory standards at the beginning and towards the end of the measurements. Drift-correction measurements were carried out on a sub-daily basis (every 6-12 hours) and several humidity-isotope response curves were performed during the study period to correct for the humidity dependency of water vapor isotopic composition. Precision of water vapor isotopic measurement are expected to be 0.14‰ for $\delta^{18}O$ and 1.1‰ for δD. The reader is referred to a previous study conducted at THMAO for additional details on calibration protocol

(Steen-Larsen et al., 2014). Humidity observations of the CRDS analyzer (moist mixing ratio, w [ppmv]) were calibrated against RH observations at the top inlet.

2.5 Estimation of evaporation flux isotopic composition

Isotopic water vapor observations acquired with CRDS analyzer represent the time-averaged atmospheric moisture composition at a certain height above sea level. We used the Keeling Plot (KP) gradient method between the two inlets to estimate the isotopic composition of the water vapor flux (δ_E). In the KP method, δ_E is assumed to be equal to the intercept of the linear best-fit model between the isotopic composition of water vapor ($\delta^{18}O$ or δD) and the inverse of humidity (1/w) at the two different height levels (Keeling, 1958). Uncertainties for δ_E were calculated as a function of instrument precision, sample size, and atmospheric conditions (Good et al., 2012). However, in our case the number of observations for each time-step is equal to the degrees of freedom required to calculate the uncertainty associated with the flux composition. Therefore, observations were grouped on a daily basis and the error on flux composition was calculated when more than two observations were available. It is important to note that the computation of flux composition with KP method is valid only under the following assumptions:

1. The mixing process in the gradient measurement space is fully turbulent and does not introduce any fractionation: turbulent diffusion is the same for all isotopologues.
2. Water vapor flux is constant with height: the mixing ratio and water vapor isotopic composition vertical profiles is characterized by a monotonic trend.
3. Variability of water vapor isotopic signal is not significantly affected by advection during the acquisition of water vapor profiles.
4. Isotopic composition of source water is constant in the time interval considered.

Therefore, water vapor observations were subset and filtered, to fulfill the above mentioned assumptions, as further discussed in Section 3.2 and Section 5.1. Because of the sensitivity to different fetch areas for the bottom and top inlets, water vapor isotopic composition at the bottom inlet was corrected ($\delta^{18}O$=+0.07‰ and δD=+0.75‰) accounting for the SST difference between open ocean SST and reef area SST, as further discussed in Section 5.2.

2.6 Estimation of non-equilibrium fractionation factors

The Craig Gordon (CG) model was used to calcuate δ_E from the ocean surface (Craig & Gordon, 1965) following the notation introduced in (Merlivat & Jouzel, 1979), as reported in equation (1):

$$\delta_E = (1-k)\frac{\alpha_{V/L}(1+\delta_L)-h(1+\delta_A)}{(1-h)} - 1 \quad (1)$$

where $\alpha_{V/L}$ [<1] is the equilibrium fractionation factor between vapor and liquid (Horita & Wesolowski, 1994), h [0-1] is the relative humidity of the free atmosphere relative to ocean surface temperature, k is the non-equilibrium fractionation factor, δ_A is the isotopic composition of atmospheric moisture, δ_L is the isotopic composition of the ocean water. The non-equilibrium fractionation factor k is estimated from a direct comparison between observed (KP) and modeled (CG) isotopic composition of the evaporation flux. For a given flux observation i, it is possible to calculate m different values of the flux composition with CG model by varying the non-equilibrium fractionation factors within a certain range. The best k values are then calculated by error minimization between modeled and observed evaporation flux composition for each pair of

top and bottom inlet observations. To estimate the average values of k, the errors of the observed flux composition were used as the weights in the computation of the average. Populations of mean non-equilibrium fractionation factors k and 95% confidence interval of the mean were estimated with bootstrapping, repeating the above sequence for 10^4 times with random resampling. Additional details on how the non-equilibrium fractionation factors are calculated are reported in Supporting Info, Text S2 and Text S3.

3 Data description

3.1 Dataset

Time series of water vapor at top and bottom inlets were resampled using a common UTC time indexing with a resolution of 30 minutes through linear interpolation. Meteorological observations were also averaged and synchronized accordingly to CRDS observations. The water vapor time series used in this study includes 8793 datapoints, representative of 30-minutes averaged observations of water vapor isotopic composition at two height levels over the ocean surface. The complete dataset accounts for 95% coverage of the study period (Figure 2).

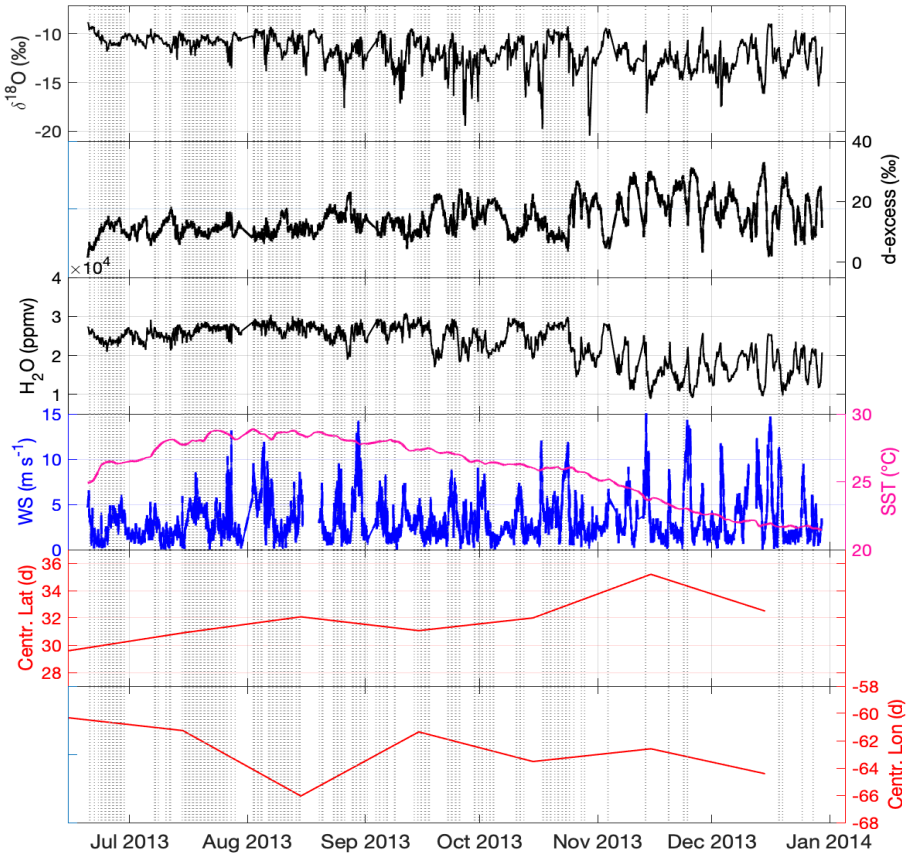

Figure 2: Timeseries of water vapor isotopic composition and relevant meteorological parameters at study site. Water vapor isotopic composition and wind speed (WS) measured at top inlet height (50 m AMSL). SST data from OSTIA. Centroid of moisture source area (latitude weighted) estimated with WaterSip. Vertical lines represent selected observations for water vapor flux estimation.

Based on d-excess, the pattern of atmospheric water vapor composition can be divided in two main groups: a first group from summer to mid-autumn with gentle daily to weekly d-excess oscillations and a second group, from mid-autumn to early winter, with larger and more pronounced d-excess oscillations at weekly scale. The transition in the d-excess pattern follows the general decrease in humidity after late October. The temperatures decrease in autumn-winter is also highlighted by the influence of different moisture sources areas, with a general shift of atmospheric water vapor origin toward the north-west (from 30 °N to 35 °N and from 60° W to 64° W, for latitude and longitude, respectively). The north-western shift in moisture sources areas highlighted here is linked to the increase in baroclinicity towards autumn and winter and to the more frequent passage of extratropical cyclones over the gulf stream (Aemisegger & Sjolte, 2018).

3.2 Filtered dataset for flux estimation

To guarantee high data quality and for maximizing the validity of assumptions under KP (Section 2.5, points 1 - 4), several constraints were introduced to filter the dataset. The rationale behind those constraints is summarized for each variable in Table 1.

Table 1: List of variables and constraints adopted to filter the time series.

Variable	Indexing	Range/Value	Rejected (cumulative)	Assumption #	Rationale
Time	Time	Daytime observations based on sunrise-sunset hour (LST) with 2 hours offset	71%	2,4	No influence of dew formation caused by night cooling.
WD	Wind sector inclusion	Western Sector 180°N – 340°N (i.e. excluding winds from inland)	85%	3,4	No influence of local evapotranspiration from vegetation
δD and $\delta^{18}O$	$\lvert\delta D_{Bottom}-\delta D_{Top}\rvert$ $\lvert\delta^{18}O_{Bottom}-\delta^{18}O_{Top}\rvert$	> 1 ‰ > 0.1 ‰	89%	2	Difference between Top/Bottom larger than instrumental precision (L2120-i)
w	$w_{Bottom} - w_{Top}$	> 100 ppmv*	89%	2	w decreases with height above ocean.
P	Time	No precipitation within the last two hours	90%	1,2,3,4	No vapor recycling from precipitation

The column "rejected" reports the size of dataset that does not fulfill each filtering threshold. Assumption n# refers to the numbered list in Section 2.5. * This is a conservative estimate of instrumental precision not reported in the L2120-I datasheet.

By means of the quality control filtering criteria, the sample size is reduced from 8793 to 814 30-minutes averaged observations (~10% of available data). The variables that are most responsible for the exclusion of data points are daytime and the western wind sector constraints. Just those two filtering criteria accounts for approximately 85% of rejections. However, this strict filtering criteria was necessary because of the strong local evapotranspiration signal developing during the night and with wind blowing from inland. The remaining filtering criteria accounted for an additional 5% of rejections.

Most of the observations (~90%) of the filtered dataset were selected between 20th June and 23th October, as shown in Figure 2. From the perspective of data representativeness, the main features of the dataset after the filtering procedure are: (i) slightly changed mean and median values (for $\delta^{18}O$ and d-excess) and reduction of secondary modes in d-excess distribution; (ii) statistically significant change in regression parameters for d-excess vs RH with respect to SST (hereafter h); (iii) significant reduction of observations charachterized by deeper PBL (PBLH > 1000 m, from 17% to 4%); (iv) change of the wind speed distribution in terms of the mean (from 2.8 ms^{-1} to 4.0 ms^{-1}). Therefore, the main consequences of data reduction are a larger impact of shallow atmospheric mixing, a smaller influence of large MBL development and lower frequency of low wind speed conditions. More details on the impact of data filtering on the distribution shape of variables of interest are reported in Supporting Info, Text S4.

4 Results

4.1 The isotopic composition of evaporation flux (δ_E) from the ocean surface

Descriptive statistics of the evaporation flux isotopic composition from the ocean surface and the water vapor isotopic composition observed at the top inlet during daytime are repoted in Table 2.

Table 2: Descriptive statistics of evaporation flux and top inlet water vapor isotopic composition at the daily timescale.

	Mean (‰)	Median (‰)	IQR (‰)	$\sigma_{\delta E}$ (‰)
Evaporation flux $\delta^{18}O$	-3.37	-4.48	-6.7 ; -0.04	1.17
Evaporation flux δD	-24.99	-33.48	-48.38 ; -1.60	7.33
Top inlet water vapor $\delta^{18}O$	-11.30	-10.97	-12.10 ; -10.51	-
Top inlet water vapor δD	-78.13	-76.14	-83.15 ; -73.10	-

On average, the number of data points available for KP calculation is 20 per day and the coefficients of determination for both $\delta^{18}O$ and δD regression lines are high ($R^2 = 0.78$, on average). For comparison, the Flux Gradient method (FG, Lee et al., 2007) was also used to compute the isotopic composition of evaporation flux, obtaining nearly identical results but different uncertainties, especially for δD ($\sigma_{\delta E}$ = 0.59‰ and 51‰ for $\delta^{18}O$ and δD, respectively). The high similarity between the FG and KP methods is consistent with other studies (Good et al., 2012; Hu et al., 2021).

As expected, the isotopic composition of the flux is enriched with respect to the atmospheric water vapor composition. The mean δD of the evaporation flux is in between recent estimates of

339 the global mean HDO cycle (-37.6‰ following Good et al., 2015) and estimates made in past
340 studies (-22‰ following e.g. Gat, 1996). No evident trend was observed for daily δ_E during the
341 study period, for both $\delta^{18}O$ and δD.

342 **4.2 Non-equilibrium fractionation factor distributions estimated with flux observations**

343 Non-equilibrium fractionation factors are expressed hereafter in term of k_{18} (for $\delta^{18}O$) and k_2 (for
344 δD) to allow a direct comparison with the parametrization of (Merlivat & Jouzel, 1979). Applying
345 the bootstrapping method with 10^4 repetitions in the filtered dataset we obtained mean ± 1 std. dev.
346 k_{18} = 5.21 ± 0.64‰ and k_2 = 4.32 ± 3.41‰, as show in Figure 3.

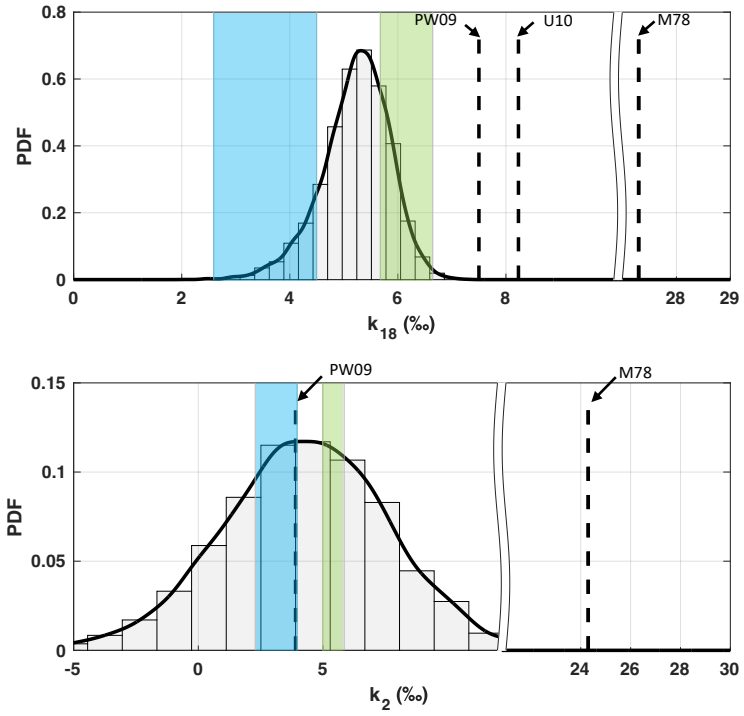

347

348 **Figure 3:** Non-equilibrium fractionation factors estimated from flux observations (KP method). Continuous kernel
349 density function was estimated with bandwidths 0.1‰ and 0.6‰ for k_{18} and k_2, respectively. Shaded area represents
350 the k intervals predicted for smooth (green, 10-m wind speed range 1-6 m s^{-1}) and rough (cyan, 10-m wind speed
351 range 6-13 m s^{-1}) regimes following Merlivat and Jouzel (1979). For reference, diffusivity ratios M78 (Merlivat,
352 1978) and non-equilibrium fractionation factors PW09 (Pfahl & Wemli, 2009) and U10 (Uemura et al., 2010) are
353 reported as vertical dashed lines.

354 The obtained k PDFs are in the range predicted by the parametrization proposed in (Merlivat &
355 Jouzel, 1979). For k_{18}, the distribution of the mean values falls in the middle of the
356 parametrizations for the smooth and rough wind speed regimes. A similar result was obtained for
357 mean k_2, which PDF is however characterized by significantly larger spread. Consistent with
358 previous works, non-equilibrium fractionation factors are on average ~0.20 - 0.25 times the value
359 expected for a purely diffusivity-driven evaporation process (Merlivat, 1978). For reference, the
360 k values estimated in other studies are also reported in Figure 3 (Pfahl & Wemli, 2009; Uemura
361 et al., 2010). Note that the k_{18} values estimated in this study are 2-3 ‰ smaller than previous
362 studies and more consistent with the parametrization of k_{18} proposed in (Merlivat & Jouzel,

1979). On average the ratio k_2/k_{18} is equal to 0.83, similar to (Merlivat & Jouzel, 1979) and (Luz et al., 2009), who also demonstrated that air temperature between 20°C and 40°C has a minimal effect on this ratio (the sensitivity is ~$5x10^{-3}$ °C^{-1}).

4.3 Observed relationship between non-equilibrium fractionation factors and 10-m wind speed

The filtered dataset was binned in 10-m wind speed classes with bin size 0.5 m s^{-1} to estimate the relationship between $k_{2,18}$ and wind speed. For each wind speed class, the non-equilibrium fractionation factors were calculated using the KP method at 30 min time step. Afterwards, mean and standard error of $k_{2,18}$ were calculated for each wind speed bin center. Mean k_{18} values obtained in such way are reported as a function of 10-m wind speed in Figure 4.a.

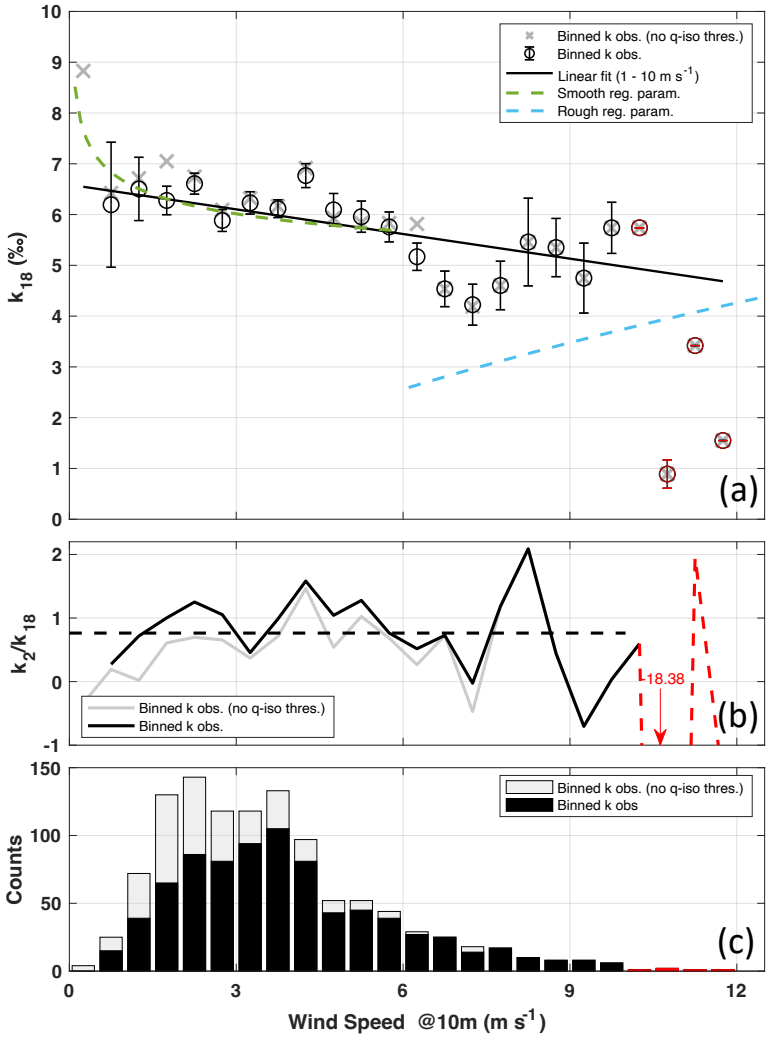

Figure 4: Observed relationship between k_{18} and 10-m wind speed. **(a)** mean ± standard error of k_{18} estimated for each wind speed class. Green and cyan lines show the parametrization of k_{18} for smooth and rough wind regimes, respectively (Merlivat & Jouzel, 1979). Solid black line represents a linear fit (R^2=0.52) in the wind speed interval 0.5 – 10 m s^{-1} (fit equation reported in text). **(b)** k_2/k_{18} ratio for each wind speed class. Dashed black line is the average ratio (0.8). **(c)** Number of observations for each bin. In all panels: black lines, black symbols and black bars for filtered dataset; gray lines, gray symbols and gray bars for filtered dataset with no isotope and humidity

thresholds implemented: red line, red symbols and red bars highlight wind speed classes with number of observation ≤ 2.

In the wind speed range [0.5 – 10] m s^{-1} the negative correlation between k_{18} and wind speed is high and statistically significant (r=-0.72, p-value=1x10^{-3}). The parametrization proposed in (Merlivat & Jouzel, 1979) predicts with good accuracy the range of observed k_{18} variability between 0.5 and 6 m s^{-1}, with an average absolute difference of 0.1‰. Most importantly, the differences between parametrized and observed k_{18} values are normally distributed around zero (Kolmogorov-Smirnov and Shapiro-Wilk p-values equals to 0.13 and 0.34, respectively) and the errors can therefore be attributed to random noise in the measurement. On the other hand, observed k_{18} are 2‰ larger than modeled k_{18} for rough regime parametrization between 6 and 10 m s^{-1}. Moreover, the theoretical wide discontinuity between smooth and rough regime expected at ~6 m s^{-1} can not be resolved. A decrease of k_{18} in the 7 ± 1 m s^{-1} wind speed region is visible but k_{18} observations quickly aligns to the main decreasing trend. The observed k_{18} values are on average 66% higher than the ones calculated with the rough regime parametrization. In other words, this study: (i) does not provide sufficient experimental evidence that there are two different regimes in the wind dependency of k_{18} and (ii) suggests that a continuous decrease of k_{18} as a function of wind speed is more likely in the interval [0.5 – 10] m s^{-1}. Such decrease can be approximated by the following simplified equation:

$$k_{18} = (-0.16 \pm 0.04) * WS + (6.6 \pm 0.3)\ ‰ \qquad (2)$$

where WS is the 10-m wind speed in m s^{-1}. Equation (2) highlights that in the wind speed range [0.5 – 10] m s^{-1} the sensitivity of k_{18} to wind speed is only -0.16 ± 0.04 ‰ m^{-1}s. Data filtering prevents to calculate k_{18} at lower wind speed values, mainly because of the threshold on humidity and isotopic composition differences between the two inlets. When such thresholds are removed, the number of observations increases on the left side of the wind speed distribution (Figure 4.c), with a ~5% increase of the sample size. Despite that enables to include steeper gradient observations, a larger uncertainty is estimated for the lowest wind speed bin (SE=1.7‰, not shown). The impact of the presence/absence of humidity and isotopic composition difference thresholds between the two inlets is minimal in the k_{18} wind speed relationship. Indeed, the average absolute difference of k_{18} with/without those thresolds is only 0.1‰ in the [0.5 – 10] m s^{-1} wind speed range, with a minimal increase of the slope of 0.04‰ m^{-1}s. Unfortunately, the limited number of datapoints above 10 m s^{-1} does not allow any other speculation on the dependency of k_{18} to higher wind speed. It is possible, however, that other processes such as sea spray contribution might start to become important in the net evaporation flux above a certain wind speed threshold (Andreas et al., 1995; Veron, 2015). Therefore, equation (2) must be considered valid only in the [0.5 – 10] m s^{-1} wind speed range.

Continuing with k_2, observations are scattered and very noisy on the k_2 vs wind speed plane (data reported in Supporting Info, Figure S5), as a result of δD less influenced by non-equilibrium fractionation than $\delta^{18}O$. The correlation between k_2 and wind speed is low and not significant within the [0.5 – 10] m s^{-1} wind speed range (r=-0.34, p-value=0.15). Observations are not in agreement with (Merlivat & Jouzel, 1979) parametrization, nor for the smooth nor for the rough regime, with an average absolute difference of 1.4‰ from the model. The noise in k_2 observations drastically affects the variability of the k_2/k_{18} ratio, which shows an average value of 0.8 and a

standard error of 0.1 (Figure 4.b). It is worth noting that the k_2/k_{18} ratio is not correlated with 10-m wind speed.

5. Discussion

5.1. Method sensitivity to filtering criteria

The KP method is based on assumptions that might not be considered always valid in a dynamic oceanic environment. Even on an island in the middle of the ocean, local evaporation sources, such as vegetation and wind direction variability, can affect the validity of a simplified binary mixing model with ocean and free atmosphere as the only end members. The strict filtering criteria used in this study to estimate the isotopic composition of the evaporation flux and the non-equilibrium fractionation factors tries to select the data for maximizing the validity of the assumptions behind an ideal binary mixing model. This strict filtering, however, reduced the original dataset size significantly, as mentioned before. Here we discuss how each filtering criteria affects the results shown in Section 4.1 - 4.3, removing only data that can be affected by moisture input from precipitation events (Figure 5).

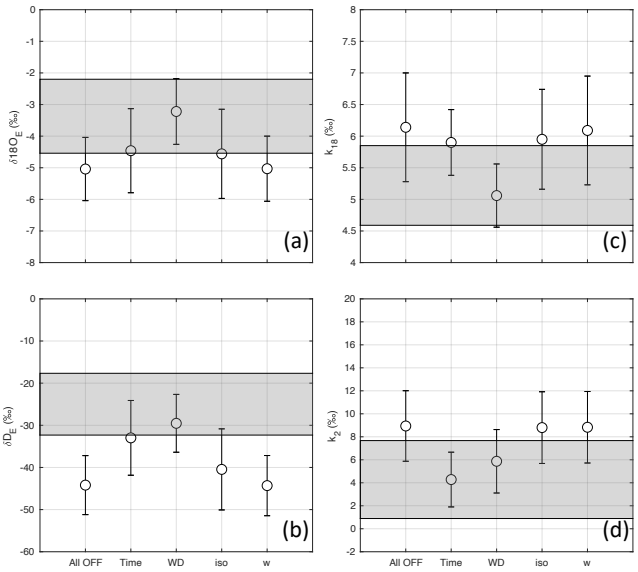

Figure 5: Sensitivity of the method for estimating δ_E and k values to filtering criteria. Following Table 1: only precitpitation filter (All off, n = 6834), time + precipitation filter (Time, n = 2016), wind sector + precipitation (WD, n = 3143), isotopic gradient + precipitation (iso, n = 3883), humidity gradient+ precipitation (w, n = 6484). **(a)** and **(b)** sensitivity of isotopic composition of evaporation flux (δ_E) for $\delta^{18}O$ and δD, respectively. **(c)** and **(d)** sensitivity of non-equilbrium fractionation factors for k_{18} and k_2, respectively. For all panels, gray shaded areas represent mean ± 1 std. deviation when enabling all filtering steps.

When all the filters are switched off, the isotopic composition of the evaporation flux decreases significantly and the mean δ_E values seem to not reflect evaporation from the ocean (Gat, 1996; Good et al., 2015; Craig & Gordon, 1965), as shown in Figure 5.a and b. Both daytime and western wind sector filters contribute enriching the isotopic composition of the flux. However, westward wind direction has the largest impact on $\delta^{18}O$ flux while daytime and westward wind

direction filtering contributes likewise on δD flux. This different impact for $\delta^{18}O$ and δD fluxes highlights the different sensitivity of the method to environmental changes in daytime-nightime temperatures (larger effect on δD, minimal on $\delta^{18}O$) and on water vapor sources (ocean source vs local evapotranspiration, similar effect for both δD and $\delta^{18}O$). The lower night temperatures, coupled to the poor ventilation due to low wind speed during the night (data not shown) increase RH substantially and enhance the contribution of local evapotranspiration. The *k* values show the mirror image of the evaporation flux composition. Indeed, wind direction filtering contributes the most on decreasing k_{18} value while time and wind direction contributes nearly equally for decreasing k_2. The steepness of isotopic and humidity gradients have only a marginal impact on the average flux composition and *k* estimation.

5.2 Impact of ocean surface composition and SST on *k* estimation

Top and bottom inlets are sensitive to different fetch areas because of the wide height gap between the two inlets at THMAO (~48 m). An analysis of the fetch areas performed with the flux footprint prediction model (Kljun et al., 2015) suggested that 90% of the fetch area for the bottom inlet is within 100 m while for top inlet is within 2800 m. Bermuda Island is characterized by shallow waters close to the coast. Therefore, it is possible that local circulation of ocean water within the reef can have an impact on SST variability and on surface water isotopic composition. Continuous measurement of SST and ocean isotopic composition covering the whole study area are not available. However, it is possible to infer the SST and salinity variability (as a proxy of evaporation) from buoys and BATS data, as shown in Figure 6.a and Figure 6.b. SST variability can be used to estimate the equilibrium water vapor variability in the

study area (Figure 6.c) while the variability of salinity can be used to estimate the variability of ocean composition (Figure 6.d).

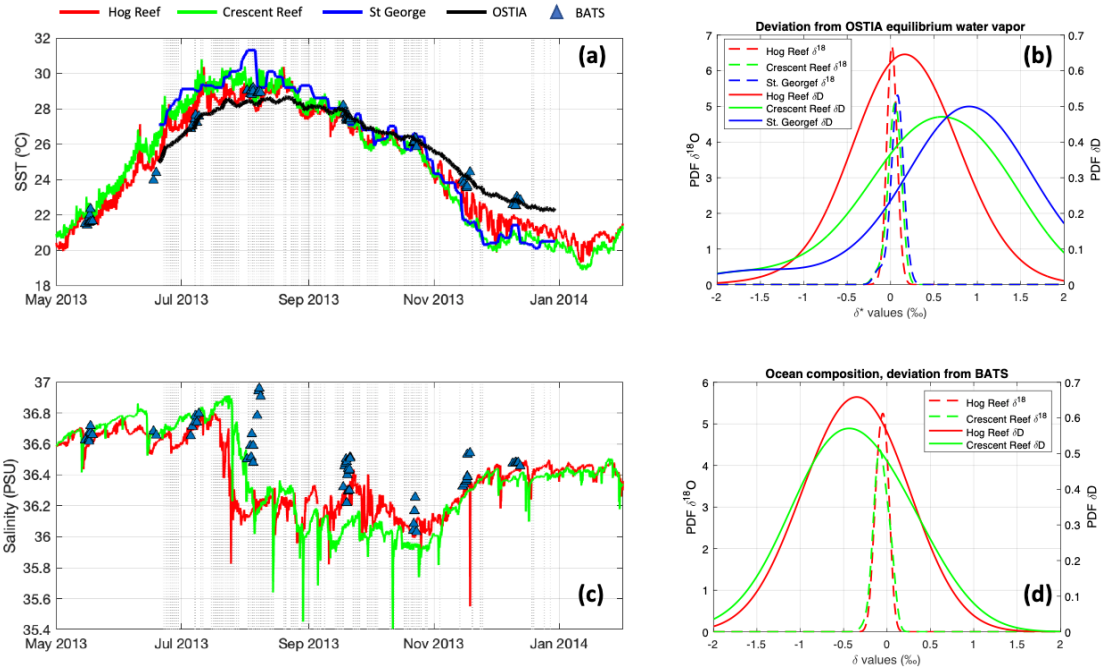

Figure 6: SST and salinity inhomogeneity of ocean waters around the study site. **(a)** Time series of SST in different points of the study area, see Figure 1 for reference of sampling sites. Vertical lines represent selected observations for flux estimation. **(b)** PDFs of [Equilibrium vapor (SST reef) – Equilibrium vapor (SST OSTIA)], where SST reef is the SST measured in different points within the reef area. **(c)** Similar to (a) but for salinity. **(d)** PDFs of [Ocean Composition (S reef) – Ocean Composition (S BATS)], where S reef is the salinity measured at different points within the reef area and S BATS is salinity measured at the BATS site. Conversion of salinity to isotopic composition following Benetti et al. (2017).

It is reasonable to assume that OSTIA SST is more representative of the isotopic composition of equilibrium water vapor for the top inlet while the SST measured within the reef is more representative for the bottom inlet. Therefore, it is possible to correct the water vapor isotopic composition at the bottom inlet by adding the mean deviation of St. George equilibrium SST from OSTIA, that is +0.07‰ and +0.75‰ for $\delta^{18}O$ and δD, respectively (i.e. the mean of blue PSD in Figure 6.b). As anticipated in Section 2.5, we used this correction to calculate the isotopic composition of evaporation fluxes shown in this study. Similarly, the ocean composition within the reef might be more representative of evaporating water within the reef, hence, an approximate offset can be added to the isotopic composition of the ocean equals to -0.06‰ and -0.38‰ for $\delta^{18}O$ and δD, respectively (i.e. the mean of the green PSD in Figure 6.d). Here we discuss how large is the impact of SST and ocean composition variability on estimation of the k values and their relationship with wind speed.

Table 3: Impact of SST and Ocean composition variability on $k_{2,18}$ and k_{18} vs wind speed parameters estimation. Uncertainies are: 0.6‰, 3.5‰, 0.04 and 0.3 for k_{18}, k_2, slope and intercept, respectively. Deviation estimated from k values obtained without any correction.

Correction	Cause	k_{18} (‰)	Dev. (%)	k_2 (‰)	Dev. (%)	k_2/k_{18}	Slope (m^{-1} s)	Interc. (‰)

No correction	-	6.0	-	12.74	-	2.11	-0.20	7.93
Salinity correction	Different isotopic composition of surface water in fetch area	5.8	-4	11.37	-11	1.96	-0.21	7.72
SST correction	SST inhomogeneity in fetch area	5.2	-14	4.32	-66	0.83	-0.16	6.59
Salinity + SST corrections	SST and surface composition inhomogeneity	5.0	-18	2.81	-78	0.57	-0.17	6.37

As shown in Table 3, the inhomogeneity of ocean composition can introduce a bias in k_{18} and k_2 in the order of 0.3‰ and 1.3‰, respectively. These biases, are smaller than the uncertainties of k_{18} and k_2. On the other hand, SST inhomogeneity in the study area can introduce a 0.8‰ and 8‰ bias in k_{18} and k_2 estimation. When the SST correction is implemented, the k_{18} bias is still comparable to k_{18} uncertainty while k_2 differs significantly when the offset is introduced (66% absolute deviation). Therefore, SST has a larger impact on δD than on $\delta^{18}O$ and the impact of ocean composition inhomogeneity in the study area is lower than the impact of SST in the estimation of k_{18} and k_2. It is worth to be noted that SST correction and Salinity + SST corrections lower the k_2/k_{18} ratio below unity (0.83 and 0.57), thus giving a physical meaning to the observation (e.g. see Table 2 in Horita et al., 2008 and reference therein). However, when both Salinity and SST corrections are implemented, k_2 resulted too low and not consistent, e.g. with recent water vapor observations in the Atlantic Ocean (Bonne et al., 2019). Finally, both corrections do not affect significantly the observed correlation between k_{18} and wind speed. The main effect of those corrections on k_{18} and k_2 is indeed to change the location of their PDFs without changing the shape of the PDF. This means that the effect introduced by the correction is translated into changing the intercept of the best fit line of Figure 4.a but keeping mostly unchanged its slope. The observed negative correlation between k_{18} and wind speed is then consistent, regardless the correction implemented.

5.3 Suggested *k* values

Given that k_{18} observations are less sensitive k_2 to spatial differences of SST, we suggest using the mean value of k_{18}=5.2‰ and k_2=4.3‰. Indeed, these *k* values are estimated using all the observations that maximized the validity of KP method assumptions and then should be representative of the mean. In General Circulation Models, k_{18} can be calculated with the observed linear relationship estimated with 10-m wind speed shown in equation (3) and k_2 can be estimated by the average observed ratio of k_2/k_{18}=0.83. These values are valid for wind speed between 0.5 and 10 m s^{-1}.

5.4 D-excess sensitivity to evaporative conditions: need for further studies

Assuming that water vapor d-excess signal is only modulated by local evaporation, the suggested non-equilibrium fractionation factors of this study can be used to predict water vapor d-excess using h (RH relative to SST) and the *Closure Assumption* (CA) (Bonne et al., 2019; Merlivat & Jouzel, 1979; Pfahl & Wernli, 2009). However, there is a significant difference between the regression parameters of the "d-excess vs h" line for CA and the observations in Bermuda (d-

excess = -36.1*h+35‰ for CA, d-excess = -46.2*h+46‰ for observations see Figure S3 in Supporting Information). In general, the mean absolute difference between d-excess estimated with CA and observed d-excess is 3.7‰. This discrepancy highlights how d-excess variability in the MBL can be affected by additional processes than humidity deficit. Atmospheric mixing between the boundary layer and the free atmosphere can be one those processes, changing the free atmosphere end member isotopic composition and, at the same time, modulating h in the MBL (Benetti et al., 2018; Risi et al., 2019). Following this idea, a simple regression model based on observed d-excess, CA and Planetary Boundary Layer height is able to reproduce 82% of the d-excess signal variability, showing that the 55% of variability can be attributed to h variability and 22% to Planetary Boundary Layer height variability. Despite the validity of CA and d-excess signal representativity in ocean water vapor is out of the scope of this study, we expect this study to highlight the needs of more research effort to determine the processes driving d-excess signal in the MBL at the daily – subdaily scale.

6 Conclusions

Profile observations of water vapor isotopic composition near the ocean surface can be used to quantify the impact of non-equilibrium effects during natural evaporation in oceanic conditions. In this study we provided a unique dataset of water vapor isotope observations collected at two different heights on a meteorological tower in Bermuda Islands, North Atlantic Ocean. Using a gradient-diffusion method we have extrapolated non-equilibrium fractionation factors distributions for $^{18}O/^{16}O$ and $^{2}H/H$ during local evaporation and their relationship with wind speed. A strict data filtering approach was used to maximize the validity of the assumptions behind the gradient-diffusion method. The main downside of this approach is a consistent reduction of the sample size but at the same time ensured a conservative approach for the estimation of non-equilibrium fractionation factors. Observed non-equilibrium fractionation factor for $^{18}O/^{16}O$ are in good agreement with smooth wind speed parametrization (mean ± 1 std.dev k_{18}=5.2 ± 0.6‰). The correlation between k_{18} and 10-m wind speed is statistically significant, with a sensitivity in the order of -0.16 to -0.20 m^{-1} s. Such low sensitivity would be nearly impossible to resolve by conventional measurements of water vapor d-excess at a single height above the ocean surface. However, the observed relationship between k_{18} and wind speed does not provide indication for the presence of a discontinuity between a smooth and rough surface under different wind regimes. We note that the original smooth-rough regime wind speed parametrization is based on the results of a single experiments at 7 m s^{-1} in Merlivat and Coantic (1975), which actually do not fit the evaporation model of Brutsaert. A monotonic decrease of k_{18} as function of wind speed is more likely for wind speeds up to 9 - 10 m s^{-1}. To this end, the rough regime parametrization of k_{18} underestimates the observed fractionation factor by 66%. Mean non-equilibrium fractionation factor for $^{2}H/H$ showed to be in the range expected by wind speed parametrization (mean ± 1 std.dev k_2=4.3 ± 3.4‰), but a larger degree of uncertainty is reported for the determination of k_2 relationship with wind speed. We showed that the spatial inhomogeneity of SST and ocean composition around the study site have a considerable impact for the estimation of k_2. On the other hand, estimation of k_{18} resulted to be consistent regardless of the strict data filtering and of the spatial variability of SST and ocean composition. We showed in addition that using the observed non-equilibrium fractionation factors with RH measurements and information of Planetary Boundary Layer height allow us to explain 82% of the water vapor d-excess variability in Bermuda. This poses the usefulness of new research effort

in understanding the physical controls of water vapor d-excess in the marine boundary layer at daily – subdaily temporal resolution.

Acknowledgments

The work was supported by the Danish Council for Independent Research – Natural Sciences grant number 10-092850 and the Carlsberg Foundation, and the AXA Research Fund. The Tudor Hill Marine Atmospheric Observatory in Bermuda is supported by NSF award OCE1829686. We acknowledge an infrastructure grant (nr. 10/0244) from the Icelandic Research Council (Rannis), that partly covered the cost of the Picarro facilities in Bermuda. HCSL and DZ acknowledges funding from the European Union's Horizon 2020 research and innovation programme under grant agreement no. 821868. H.S. acknowledges support by the Norwegian Research Council (Project SNOWPACE, grant no. 262710) and by the European Research Council (Consolidator Grant ISLAS, project no. 773245). SW acknowledges funding from the European Research Council (ERC) under the European Union's Horizon 2020 research and innovation program: Starting Grant-SNOWISO (grant agreement 759526).

Open Research

The water vapor and meteorological time series used for calculating the non-equilibrium fractionation factors in the study will be uploaded on Pangea, DOI to be minted with CC BY 4.0. Code for data analysis and for reproducing plots in the article is available at corresponding author repository: https://github.com/danielez83/Bermuda-NEFF

References

Aemisegger, F., & Sjolte, J. (2018). A climatology of strong large-scale ocean evaporation events. Part II: Relevance for the deuterium excess signature of the evaporation flux. *Journal of Climate*, *31*(18), 7313–7336. https://doi.org/10.1175/JCLI-D-17-0592.1

Andreas, E. L., Edson, J. B., Monahan, E. C., Rouault, M. P., & Smith, S. D. (1995). The spray contribution to net evaporation from the sea: A review of recent progress. *Boundary-Layer Meteorology*, *72*(1–2), 3–52. https://doi.org/10.1007/BF00712389

Benetti, M., Lacour, J. L., Sveinbjörnsdóttir, A. E., Aloisi, G., Reverdin, G., Risi, C., et al. (2018). A Framework to Study Mixing Processes in the Marine Boundary Layer Using Water Vapor Isotope Measurements. *Geophysical Research Letters*, *45*(5), 2524–2532. https://doi.org/10.1002/2018GL077167

Benetti, Marion, Reverdin, G., Pierre, C., Merlivat, L., Risi, C., Steen-larsen, H. C., & Vimeux, F. (2014). Deuterium excess in marine water vapor: Dependency on relative humidity and surface wind speed during evaporation, 584–593. https://doi.org/10.1002/2013JD020535.Received

Benetti, Marion, Reverdin, G., Aloisi, G., & Sveinbjörnsdóttir, Á. (2017). Stable isotopes in surface waters of the A tlantic O cean: Indicators of ocean-atmosphere water fluxes and oceanic mixing processes. *Journal of Geophysical Research: Oceans*, *122*(6), 4723–4742.

BIOS. (2021). Bermuda Atlantic Time-series Study (BATS).

Bonne, J. L., Behrens, M., Meyer, H., Kipfstuhl, S., Rabe, B., Schönicke, L., et al. (2019). Resolving the controls of water vapour isotopes in the Atlantic sector. *Nature Communications*, *10*(1), 1–10. https://doi.org/10.1038/s41467-019-09242-6

Ciais, P., & Jouzel, J. (1994). Deuterium and oxygen 18 in precipitation: isotopic model, including mixed cloud processes. *Journal of Geophysical Research*, *99*(D8). https://doi.org/10.1029/94jd00412

Craig, H. (1961). Isotopic variations in meteoric waters. *Science*, *133*(3465), 1702–1703.

Dansgaard, W. (1964). Stable isotopes in precipitation. *Tellus*, *16*(4), 436–468. https://doi.org/10.3402/tellusa.v16i4.8993

Dee, D. P., Uppala, S. M., Simmons, A. J., Berrisford, P., Poli, P., Kobayashi, S., et al. (2011). The ERA-Interim reanalysis: Configuration and performance of the data assimilation system. *Quarterly Journal of the Royal Meteorological Society*, *137*(656), 553–597. https://doi.org/10.1002/qj.828

Faber, A.-K., Steen-Larsen, H. C., & Sodemann, H. (2020). Revisiting the origin of Greenland moisture sources: Regional differences, seasonality and land/ocean sources. In *AGU Fall Meeting Abstracts* (Vol. 2020, pp. C033--06).

Galewsky, J., Steen-Larsen, H. C., Field, R. D., Worden, J., Risi, C., & Schneider, M. (2016). Stable isotopes in atmospheric water vapor and applications to the hydrologic cycle. *Reviews of Geophysics*, *54*(4), 809–865. https://doi.org/10.1002/2015RG000512

Galewsky, J., Jensen, M. P., & Delp, J. (2022). Marine Boundary Layer Decoupling and the Stable Isotopic Composition of Water Vapor. *Journal of Geophysical Research: Atmospheres*, *127*(3), 1–14. https://doi.org/10.1029/2021jd035470

Gat, J. R. (1996). Oxygen and Hydrogen Isotopes in the Hydrologic Cycle. *Annual Review of Earth and Planetary Sciences*, *24*(1), 225–262. https://doi.org/10.1146/annurev.earth.24.1.225

Gat, J. R., Klein, B., Kushnir, Y., Roether, W., Wernli, H., Yam, R., & Shemesh, A. (2003). Isotope composition of air moisture over the Mediterranean Sea: An index of the air-sea interaction pattern. *Tellus, Series B: Chemical and Physical Meteorology*, *55*(5), 953–965. https://doi.org/10.1034/j.1600-0889.2003.00081.x

Gonfiantini, R., Wassenaar, L. I., & Araguas-Araguas, L. J. (2020). Stable isotope fractionations in the evaporation of water: The wind effect. *Hydrological Processes*, *34*(16), 3596–3607. https://doi.org/10.1002/hyp.13804

Good, S. P., Soderberg, K., Wang, L., & Caylor, K. K. (2012). Uncertainties in the assessment of the isotopic composition of surface fluxes: A direct comparison of techniques using laser-based water vapor isotope analyzers. *Journal of Geophysical Research Atmospheres*, *117*(15), 1–22. https://doi.org/10.1029/2011JD017168

Good, S. P., Noone, D., Kurita, N., Benetti, M., & Bowen, G. J. (2015). D/H isotope ratios in the global hydrologic cycle. *Geophysical Research Letters*, *42*(12), 5042–5050. https://doi.org/10.1002/2015GL064117

Griffis, T. J., Wood, J. D., Baker, J. M., Lee, X., Xiao, K., Chen, Z., et al. (2016). Investigating the source, transport, and isotope composition of water vapor in the planetary boundary layer. *Atmospheric Chemistry and Physics*, *16*(8), 5139–5157. https://doi.org/10.5194/acp-16-5139-2016

H Craig, & Gordon, L. I. (1965). *Stable Isotopes in Oceanographic Studies and paleotemperatures*.

Held, I. M., & Soden, B. J. (2000). Water Vapor Feedback and Global Warming. *Annual Review of Energy and the Environment*, *25*, 441–475.

Hersbach, H., Bell, B., Berrisford, P., Hirahara, S., Horányi, A., Muñoz-Sabater, J., et al. (2020). The ERA5 global reanalysis. *Quarterly Journal of the Royal Meteorological Society*,

146(730), 1999–2049. https://doi.org/10.1002/qj.3803
Hijmans, R. J. (2015). Boundary, Bermuda, 2015. Retrieved from https://maps.princeton.edu/catalog/stanford-nw036zp7611
Horita, J., & Wesolowski, D. J. (1994). Liquid-vapor fractionation of oxygen and hydrogen isotopes of water from the freezing to the critical temperature. *Geochimica et Cosmochimica Acta*, *58*(16), 3425–3437. Retrieved from papers2://publication/uuid/F9BCD32F-8569-4ACF-81AF-08518BF40A32
Horita, J., Rozanski, K., & Cohen, S. (2008). Isotope effects in the evaporation of water: A status report of the Craig-Gordon model. *Isotopes in Environmental and Health Studies*, *44*(1), 23–49. https://doi.org/10.1080/10256010801887174
Hu, Y., Xiao, W., Wei, Z., Welp, L. R., Wen, X., & Lee, X. (2021). Determining the Isotopic Composition of Surface Water Vapor Flux From High-Frequency Observations Using Flux-Gradient and Keeling Plot Methods. *Earth and Space Science*, *8*(3), 1–15. https://doi.org/10.1029/2020EA001304
IAEA. (2009). Reference sheet for international measurement standards - SMOW Vienna Standard Mean Ocean.
Johnsen, S. J., Dansgaard, W., & White, J. W. C. (1989). The origin of Arctic precipitation under present and glacial conditions. *Tellus, Series B*, *41 B*(4), 452–468. https://doi.org/10.3402/tellusb.v41i4.15100
Jouzel, J., Stiévenard, M., Johnsen, S. J., Landais, A., Masson-Delmotte, V., Sveinbjornsdottir, A., et al. (2007). The GRIP deuterium-excess record. *Quaternary Science Reviews*, *26*(1–2), 1–17. https://doi.org/10.1016/j.quascirev.2006.07.015
Keeling, C. D. (1958). The concentration and isotopic abundances of atmospheric carbon dioxide in rural areas. *Geochimica et Cosmochimica Acta*, *13*, 322–324. Retrieved from papers2://publication/uuid/A28C5407-A4A1-4D85-9BA9-589DE73CD49C
Kljun, N., Calanca, P., Rotach, M. W., & Schmid, H. P. (2015). A simple two-dimensional parameterisation for Flux Footprint Prediction (FFP). *Geoscientific Model Development*, *8*(11), 3695–3713. https://doi.org/10.5194/gmd-8-3695-2015
Lee, X., Kim, K., & Smith, R. (2007). Temporal variations of the 18O/16O signal of the whole-canopy transpiration in a temperate forest. *Global Biogeochemical Cycles*, *21*(3), 1–12. https://doi.org/10.1029/2006GB002871
LeGrande, A. N., & Schmidt, G. A. (2006). Global gridded data set of the oxygen isotopic composition in seawater. *Geophysical Research Letters*, *33*(12), 1–5. https://doi.org/10.1029/2006GL026011
Luz, B., Barkan, E., Yam, R., & Shemesh, A. (2009). Fractionation of oxygen and hydrogen isotopes in evaporating water. *Geochimica et Cosmochimica Acta*, *73*(22), 6697–6703. https://doi.org/10.1016/j.gca.2009.08.008
Markle, B. R., Steig, E. J., Roe, G. H., Winckler, G., & McConnell, J. R. (2018). Concomitant variability in high-latitude aerosols, water isotopes and the hydrologic cycle. *Nature Geoscience*, *11*(11), 853–859. https://doi.org/10.1038/s41561-018-0210-9
Merlivat, L., & Coantic, M. (1975). Study of mass transfer at the air-water interface by an isotopic method. *Journal of Geophysical Research*, *80*(24), 3455–3464. https://doi.org/10.1029/jc080i024p03455
Merlivat, Liliane. (1978). Molecular diffusivities of H 2 16 O, HD 16 O, and H 2 18 O in gases. *The Journal of Chemical Physics*, *69*(6), 2864–2871.
Merlivat, Liliane, & Jouzel, J. (1979). Global climatic interpretation of the deuterium-oxygen 18

relationship for precipitation. *Ournal of Geophysical Research: Oceans*, *84*(C8), 5029–5033.

NOAA. (2019). Bermuda 1 arc-second Coastal Digital Elevation Model. Retrieved from https://www.ncei.noaa.gov/metadata/geoportal/rest/metadata/item/gov.noaa.ngdc.mgg.dem:5010/html

Pfahl, S., & Sodemann, H. (2014). What controls deuterium excess in global precipitation? *Climate of the Past*, *10*(2), 771–781. https://doi.org/10.5194/cp-10-771-2014

Pfahl, Stephan, & Wernli, H. (2009). Lagrangian simulations of stable isotopes in water vapor: An evaluation of nonequilibrium fractionation in the Craig-Gordon model. *Journal of Geophysical Research Atmospheres*, *114*(20), 1–12. https://doi.org/10.1029/2009JD012054

Pfahl, Stephan, & Wernli, H. (2008). Air parcel trajectory analysis of stable isotopes in water vapor in the eastern Mediterranean. *Journal of Geophysical Research Atmospheres*, *113*(20), 1–16. https://doi.org/10.1029/2008JD009839

Risi, C., Noone, D., Frankenberg, C., & Worden, J. (2013). Role of continental recycling in intraseasonal variations of continental moisture as deduced from model simulations and water vapor isotopic measurements. *Water Resources Research*, *49*(7), 4136–4156. https://doi.org/10.1002/wrcr.20312

Risi, C., Galewsky, J., Reverdin, G., & Brient, F. (2019). Controls on the water vapor isotopic composition near the surface of tropical oceans and role of boundary layer mixing processes. *Atmospheric Chemistry and Physics*, *19*(19), 12235–12260. https://doi.org/10.5194/acp-19-12235-2019

Rozanski, K., Araguás-Araguás, L., & Gonfiantini, R. (1993). Isotopic Patterns in Modern Global Precipitation. *Geophysical Monograph*, *78*, 1–36. https://doi.org/10.1029/gm078p0001

Sodemann, H., Schwierz, C., & Wernli, H. (2008). Interannual variability of Greenland winter precipitation sources: Lagrangian moisture diagnostic and North Atlantic Oscillation influence. *Journal of Geophysical Research Atmospheres*, *113*(3), 1–17. https://doi.org/10.1029/2007JD008503

Sodemann, Harald, & Läderach, A. (2021). WaterSip. Retrieved from https://wiki.uib.no/gfi/index.php/WaterSip

Steen-Larsen, H. C., Masson-Delmotte, V., Sjolte, J., Johnsen, S. J., Vinther, B. M., Bréon, F. M., et al. (2011). Understanding the climatic signal in the water stable isotope records from the NEEM shallow firn/ice cores in northwest Greenland. *Journal of Geophysical Research Atmospheres*, *116*(6), 1–20. https://doi.org/10.1029/2010JD014311

Steen-Larsen, H. C., Sveinbjörnsdottir, A. E., Peters, A. J., Masson-Delmotte, V., Guishard, M. P., Hsiao, G., et al. (2014). Climatic controls on water vapor deuterium excess in the marine boundary layer of the North Atlantic based on 500 days of in situ, continuous measurements. *Atmospheric Chemistry and Physics*, *14*(15), 7741–7756. https://doi.org/10.5194/acp-14-7741-2014

Steen-Larsen, H. C., Sveinbjörnsdottir, A. E., Jonsson, T., Ritter, F., Bonne, J. -L., Masson-Delmotte, V., et al. (2015). Moisture sources and synoptic to seasonal variability of North Atlantic water vapor isotopic composition. *Journal of Geophysical Research Atmospheres*, *120*. https://doi.org/10.1002/2015JD023234

Stewart, M. K. (1975). Stable isotope fractionation due to evaporation and isotopic exchange of falling waterdrops: Applications to atmospheric processes and evaporation of lakes. *Journal of Geophysical Research*, *80*(9), 1133–1146. https://doi.org/10.1029/jc080i009p01133

Stull, R. B. (1997). *An Introduction to Boundary Layer Meteorology*. Springer.

Thurnherr, I., Kozachek, A., Graf, P., Weng, Y., Bolshiyanov, D., Landwehr, S., et al. (2020). Meridional and vertical variations of the water vapour isotopic composition in the marine boundary layer over the Atlantic and Southern Ocean. *Atmospheric Chemistry and Physics*, *20*(9), 5811–5835. https://doi.org/10.5194/acp-20-5811-2020

Uemura, R., Matsui, Y., Yoshimura, K., Motoyama, H., & Yoshida, N. (2008). Evidence of deuterium excess in water vapor as an indicator of ocean surface conditions. *Journal of Geophysical Research Atmospheres*, *113*(19), 1–10. https://doi.org/10.1029/2008JD010209

Uemura, R., Barkan, E., Abe, O., & Luz, B. (2010). Triple isotope composition of oxygen in atmospheric water vapor. *Geophysical Research Letters*, *37*(4), 1–4. https://doi.org/10.1029/2009GL041960

UK MET OFFICE. (2005). OSTIA L4 SST Analysis. Ver. 1.0. PO.DAAC. https://doi.org/https://doi.org/10.5067/GHOST-4FK01

Veron, F. (2015). Ocean spray. *Annual Review of Fluid Mechanics*, *47*, 507–538. https://doi.org/10.1146/annurev-fluid-010814-014651

Journal of Geophysical Research: Atmospheres

Supporting Information for

$^{2}H/H$ and $^{18}O/^{16}O$ Non-Equilibrium Fractionation Factors for Ocean Evaporation in the North-West Atlantic Region

D. Zannoni[1], H. C. Steen-Larsen[1], A. J. Peters[2], S. Wahl[1], H. Sodemann[1] and A. E. Sveinbjörnsdóttir[3]

[1]Geophysical Institute, University of Bergen and Bjerknes Centre for Climate Research, 5007, Bergen, NORWAY.

[2]Bermuda Institute of Ocean Sciences, St. George's GE01, BERMUDA.

[3]Institute of Earth Sciences, University of Iceland, Reykjavik, ICELAND.

Contents of this file

Introduction

In this Supporting Information file are reported all the additional explanations, table and figures regarding methods and results that are not critical for the outcome of the main manuscript but might help providing a clearer picture of the study to the reader. In order, the supporting file includes:

Text S1, Table S1: Values and references used to estimate the isotopic composition of the ocean around Bermuda

Text S2, Figure S1: Explanation of the Craig Gordon model focusing on non-equilibrium fractionation factors.

Text S3: Explanation of the algorithm used to estimate non-equilibrium fractionation factors

Text S4, Figures S2 – S4: Effect of data filtering on PDFs of main variables

Figure S5: scatterplot of k_2 vs 10-m wind speed

Text S1: Isotopic composition of the ocean.

No measurements of ocean water isotopic composition near the study site are available for the time period of interest. However, the temporal variability of ocean isotopic composition in the study area is expected to be very low. Several sources have been considered to estimate the most representative composition of ocean water around the study site: gridded dataset, North Atlantic cruises published data as well as from samples collected at the Bermuda Atlantic Time-series Study (BATS) site during 2012. Details for these datasets are briefly reported in **Error! Reference source not found.**. $\delta^{18}O$, δD and S data from BATS cruises for summer 2012 are fully comparable with Western North Atlantic Ocean data for summer 2015 and 2016 around Bermuda area and with Eastern North Atlantic Ocean data for summer 2012. All $\delta^{18}O$ observations reported in **Error! Reference source not found.** are more enriched than in gridded dataset[3], but still comparable when considering uncertainties. We calculated the isotopic composition of ocean water for this study combining salinity measurements performed during the study period (Hog Reef, Crescent Reef and BATS) and δ vs S relationship[5] and BATS 2012 data. This approach gives us an interval for ocean water isotopic composition in the study area (last line in **Error! Reference source not found.**). The average isotopic composition of the ocean in this study is then assumed to be $\delta^{18}O_L$= 1.09‰ and δD_L = 7.25‰ (d-excess = -1.47).

Table S1: Isotopic composition and salinity for North Atlantic Ocean.

Source	$\delta^{18}O$ ± 1SD (‰)	δD + 1SD (‰)	d-excess (‰)	Salinity (PSU)	Details
BATS, 2012 (BIOS, 2021)	1.27 ± 0.07 [0.39 S – 13.1‰]	7.92 ± 0.81 [8.64 S – 307.6]	-2.22	36.55	BATS cruises: May – Sept 2012
(Marion Benetti et al., 2014)	1.24 ± 0.09 [0.28 S – 9.0‰]	8.18 ± 0.65 [1.58 S – 50.6‰]	-1.72	37.03	Strasse Cruise: Aug – Sept 2012 Eastern N. Atlantic
(Marion Benetti et al., 2017)	1.19 ± 0.12 [0.32 S – 10.5‰]	8.03 ± 0.81 [2.04 S – 65.8‰]	-1.51	36.22	Rara Cruise: Mar and May 2015 Colibri Cruise: Aug 2016 Leg in Bermuda area
(LeGrande & Schmidt, 2006)	1.07 ± 0.15 [0.55 S – 18.98‰]	-	-	-	Averaged in a 10°x10° centered in Bermuda
Average in Bermuda Area	1.23	7.97	-0.51	36.39	BATS, 2012 Benetti et al., 2017
Estimated from δ vs S	1.12* 1.06†	8.29* 6.20†	-0.67* -2.28†	36.32	June – Dec 2013

[δ vs S linear relationship]. δ vs S relationship for N. Atlantic (Marion Benetti et al., 2017): *Using δ vs S in for gridded dataset (LeGrande & Schmidt, 2006). †Using δ vs S estimated from *BIOS* (BIOS, 2021).

Text S2: Details on Craig Gordon (CG) model and non-equilibrium fractionation

The CG model can be parametrized into a five layers process, as shown in Figure S1, with an atmospheric component based on the Langmuir linear-resistance model for evaporation where transport of water molecules can be defined as a resistance to atmospheric transport. Starting from the bottom, the first layer is well-mixed ocean water. The second layer is the interface between water and air. Here, humidity is at saturation (h = 1) and equilibrium fractionation is assumed to be reached. The third layer is a diffusion-controlled layer where different water isotopologues are characterized by different diffusivities in air. The fourth layer is a turbulence-controlled layer. In this fourth layer, no isotopic fractionation occurs because all water isotopologues of water are characterized by identical mixing behavior. The fifth layer is the "Free atmosphere", where humidity and isotopologues profiles become less pronounced with height. The actual size of the layers 2-3-4 depends on location, time of the day and atmospheric conditions. However, it is expected that layers 2 and 3 are extremely thin and very hard to resolve with current measurement techniques (Madsen et al., 2019). Measurements above the ocean surface, like in this study, predominantly take place in the fifth or within the fourth layer (top and bottom inlet in Figure S1) making the abovementioned assumption "*The mixing process in the gradient measurement space is fully turbulent and does not introduce any fractionation*" reasonable.

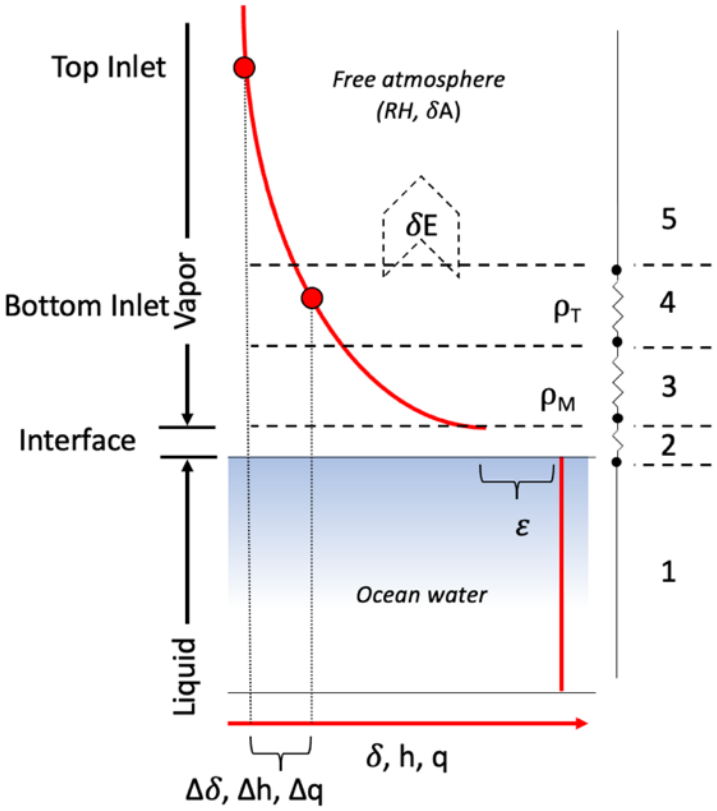

Figure S1: Visual representation of Craig-Gordon model with reference to measurement point of the THMAO tower. Layer size and sampling inlet heights are not to scale.

The non-equilibrium fractionation (k) depends on the ratio between turbulent an molecular transport and the diffusivities of different isotopologues in air, as defined in (Merlivat & Jouzel, 1979):

$$\boldsymbol{k} = \frac{\left(\frac{D}{D_i}\right)^{n} - 1}{\left(\frac{D}{D_i}\right)^{n} + \frac{\rho_T}{\rho_M}} \quad \text{(eq. S1)}$$

where the ratio D/D_i is the ratio between diffusivities of the rare isotopologue of water *i* and the common isotopologue of water; the exponent *n* depends on the wind regime and is equal to 2/3 and to 1/2 for smooth and rough wind regimes; ρ_T and ρ_M are the resistances relative to turbulent and molecular transport in air, respectively. In the Brutsaert evaporation model, the ratio of resistances can be estimated for smooth and rough surfaces with equations S2 and S3 (Brutsaert, 1965):

$$\frac{\rho_T}{\rho_M} = \frac{1}{\chi} \frac{ln\left(\frac{u_* z}{30\nu}\right)}{13.6\left(\frac{\nu}{D}\right)^{n}} \quad \text{(eq. S2)}$$

$$\frac{\rho_T}{\rho_M} = \frac{1}{\chi} \frac{ln\left(\frac{z}{z_0}\right) - 5}{7.3 R_{es}^{1/4}\left(\frac{\nu}{D}\right)^{n}} \quad \text{(eq. S3)}$$

where χ is Von Karman constant; u_* is the friction velocity [m s^{-1}]; ν is the kinematic air viscosity [kg m^{-1} s^{-1}]; *z* is the height above the water surface [m]; z_0 is the roughness length [m]; R_{es} is the surface roughness Reynolds number [-]. Therefore, the fractionation factor *k* can be directly calculated as a function of wind speed *u* [m s^{-1}] at a reference level (e.g. 10 m) because:

$$\boldsymbol{u_*} = \frac{\chi u}{ln\left(\frac{z}{z_0}\right)} \quad \text{(eq. S4)}$$

$$\boldsymbol{R_{es}} = \frac{u_* z_0}{\nu} \quad \text{(eq. S5)}$$

It has been proposed that equation S2 is valid when $R_{es} < 1$ and equation S3 when $R_{es} > 1$ (Merlivat, 1978). This variation of transport regime produces a discontinuity in the *k* vs wind speed relationship. Such discontinuity for 10m wind speed is ≈ 6 m s^{-1}.

Text S3: Algorithm for choosing the best *k* value

Non-equilibrium fractionation factor *k* is estimated from a direct comparison between observed and modeled isotopic composition of evaporation flux. For a given flux observation *i*, it is possible to calculate *m* different values of flux composition with CG model by varying the kinetic fractionation factors within a certain range. Then, applying the same procedure to all the n-observations available, it is possible to obtain a *n x m* matrix that can be compared to observed flux in the following way:

$$\overline{\boldsymbol{DF}}_{(\boldsymbol{n\,x\,m})} = \left(\overline{\boldsymbol{CG}} - \overline{\boldsymbol{\delta}}_{\boldsymbol{E}}\right)^{\circ 2} \quad \text{(eq. S6)}$$

where the matrix $\overline{\boldsymbol{\delta}}_{\boldsymbol{E}}$ is composed by the column vector of observed flux isotopic composition concatenated *m* times. Then, the differences between modeled and observed values are squared (Hadamard power) and the minimum difference for each observation can be calculated as follows:

$$\overline{\boldsymbol{min}}_{\boldsymbol{n\,x\,1}} = \min_{\boldsymbol{j \in J}}\left(\overline{\boldsymbol{DF}}\right), \ \forall \boldsymbol{i} \in \boldsymbol{I} \quad \text{(eq. S7)}$$

being I [$1,\ldots,i,\ldots,n$] and J [$1,\ldots,j,\ldots,m$] the indices of the rows and columns of the matrix $\overline{\boldsymbol{DF}}$, respectively. Similarly, the vector of minimum differences can be concatenated m times to obtain the matrix $\overline{\boldsymbol{MIN}}_{\boldsymbol{n\,x\,m}}$ that can be compared with $\overline{\boldsymbol{DF}}$ to obtain a weighting matrix $\overline{\boldsymbol{BM}}$:

$$\overline{\boldsymbol{BM}}_{(\boldsymbol{n\,x\,m})} = \overline{\boldsymbol{DF}} == \overline{\boldsymbol{MIN}} \qquad \text{(eq. S8)}$$

where the double equal in equation S8 is used to distinguish Boolean equality comparison from variable assignation. The $\overline{\boldsymbol{BM}}$ matrix identify the elements of $\overline{\boldsymbol{CG}}$ that best match the observed isotopic composition of evaporation flux by minimization of the differences and, as a direct consequence, the best kinetic fractionation value for each observation ($\overline{\boldsymbol{BK}}_{\boldsymbol{n\,x\,1}}$). The mean kinetic fractionation value k then can be estimated with a weighted average using the error on flux composition ($\boldsymbol{\sigma E_i}$) as the weight:

$$\boldsymbol{k} = \sum_{\boldsymbol{i=1}}^{\boldsymbol{n}} \boldsymbol{w_i} * \boldsymbol{BK_i}, \qquad \boldsymbol{w_i} = \frac{\left|\frac{\boldsymbol{\sigma E_i}}{\boldsymbol{\delta E_i}}\right|}{\sum_{\boldsymbol{i=1}}^{\boldsymbol{n}} \left|\frac{\boldsymbol{\delta E_i}}{\boldsymbol{\sigma E_i}}\right|} \quad \text{(eq13)}$$

Text S4: Impact of data filtering on observations PDFs

After data filtering, top inlet $\delta^{18}O$ data distribution becomes less affected by depleted values maintaining approximately unchanged its mean and median values (mean = median ≈ -11‰ prior and after data filtering with a standard deviation of 1‰). The change in distribution shape is more appreciable for d-excess, where data filtering reduced the magnitude of secondary modes (see Figure S1 for $\delta^{18}O$ and d-excess).

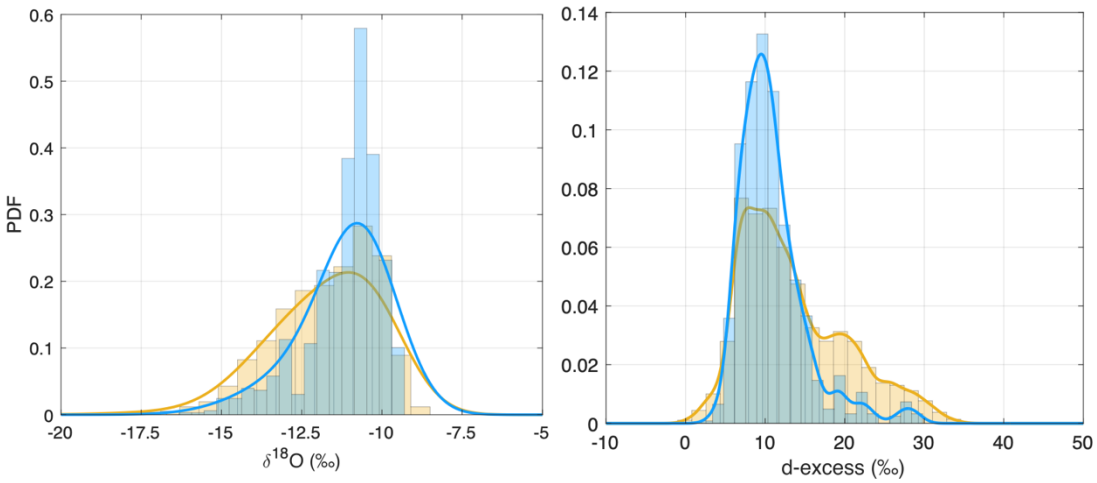

Figure S2: Distribution of water vapor isotopic composition prior (orange) and after data filtering (blue) for Top inlet. A continuous kernel density function was estimated with bandwidth = 1‰.

Presence of several modes in d-excess can be attributed to concurrence of different process involved in water vapor d-excess signal such as change in moisture source area, rain droplets evaporation and increased influence of entrainment. After data filtering, d-excess mean ± 1 standard deviation lowered from 15 ± 6 ‰ to 12 ± 4 ‰.

Correlation between water vapor d-excess and h (RH relative to SST) is very high in Bermuda (R=-0.91, for all top inlet observations). However, dataset reduction lowered the linear regression

coefficients significantly, from -48 %/‰ to -46 %/‰ and from 48 ‰ to 46 ‰, for slope and intercept, respectively (Figure S3).

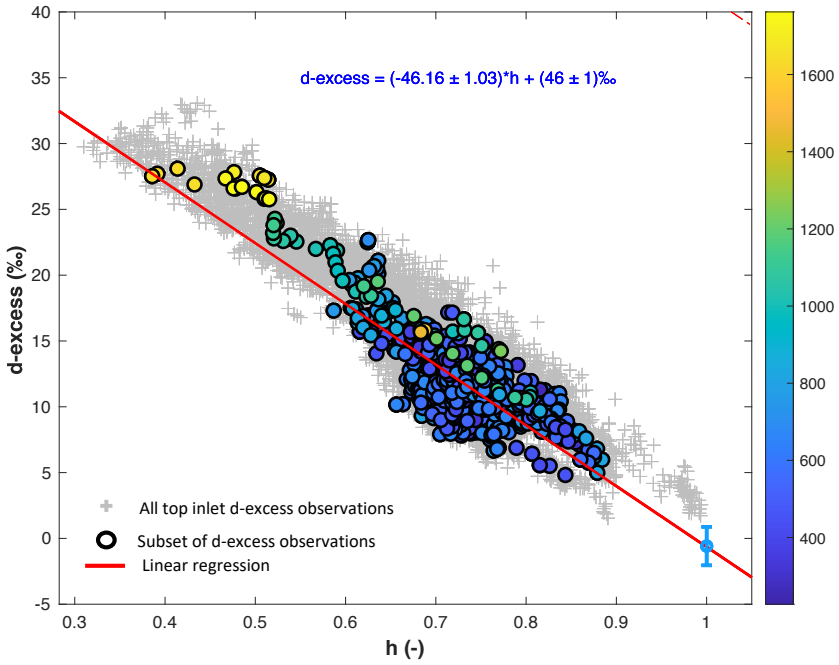

Figure S3: Relationship between d-excess, h and BLH. Colored circles represent reduced dataset observations from the top inlet observations after data reduction. D-excess of water vapor in isotopic equilibrium with ocean water is -0.8 ± 0.7‰, estimated with ocean water composition $\delta^{18}O_L$ = 1.09 ± 0.03‰, δD_L =7.25 ± 1.05‰ and mean SST = 25.9°C. Linear regression was calculated for reduced data (R^2 = 0.70).

The linear regression models between h and d-excess is able to reproduce the estimated d-excess of water vapor in isotopic equilibrium with ocean water. The predicted d-excess at h=1 resulted -0.31‰ and -0.34‰ for full and filtered dataset, respectively. Previous long-term water vapor observations in Bermuda showed that variability on regression parameters are linked to season and to wind direction (Steen-Larsen et al., 2015). Moreover, as recently pointed out in (Benetti et al., 2018), mixing with upper tropospheric air and planetary boundary layer thickness play an important role in water vapor d-excess variability in the North Atlantic. Bermuda d-excess is highly correlated with BLH (R=0.74) and the correlation is still high after data reduction (R=0.63).

Typical fully developed boundary layer height is 800 m at 15:00 (LST) which tends to increase from November and later on (1100 m, centered between 12:00 and 15:00 LST). However, the number of observations characterized by large BLH values (> 1100 m) was significantly reduced after data filtering (Figure S4), from ~17% to ~4%.

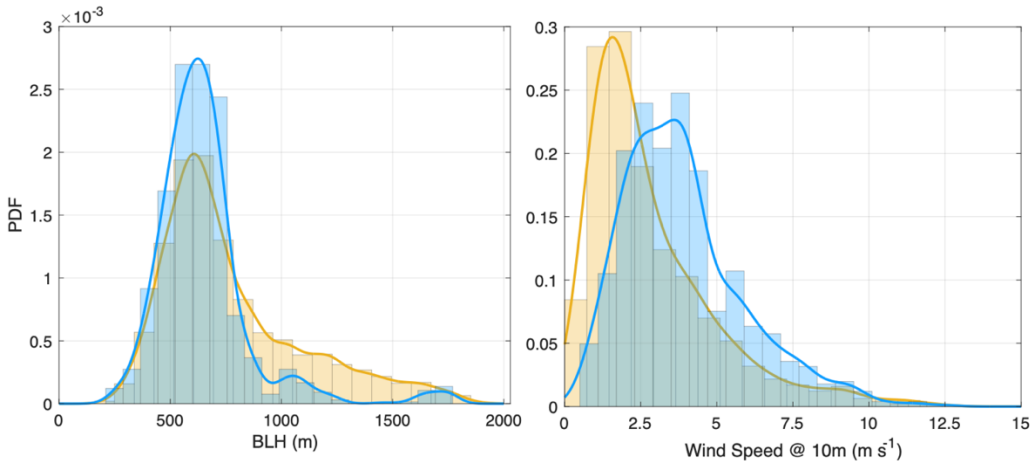

Figure S4: Distribution of BLH and WS datasets prior (orange) and after data reduction (blue). A continuous kernel density function was estimated with bandwidth = 50 m and 0.5 ms^{-1} for BLH and WS, respectively. WS was corrected to 10m height.

The main mode, the mean, and the median of BLH does not change significantly after data filtering (from 607 m, 777 m, 679 m to 623 m, 646 m, 620 m for mode, mean and median, respectively). Bottom and top inlet heights are within 1/10 of BLH in 80% of the cases. Therefore, most of the observations can be assumed to be performed within the surface layer, assuming the surface layer height to be roughly the bottom 10% of the BLH (Geernaert, 2003). On the contrary, data filtering significantly affected the wind speed distribution at the study site, largely reducing the number of observations characterized by low wind speed. The distribution shape after data reduction cannot still be considered of the normal-type but still of the Weibull-type. However, skewness reduced from 1.6 to 0.96 with mode, mean and median of WS changed from 1.6 ms^{-1}, 2.8 ms^{-1}, 2.2 ms^{-1} to 3.6 ms^{-1}, 4.0 ms^{-1}, 3.7 ms^{-1}. Therefore, the main consequence of data reduction from the perspective of d-excess sensitivity to ocean surface condition is a larger impact of shallow mixing with lesser influence on large marine boundary layer development and on low wind speed conditions.

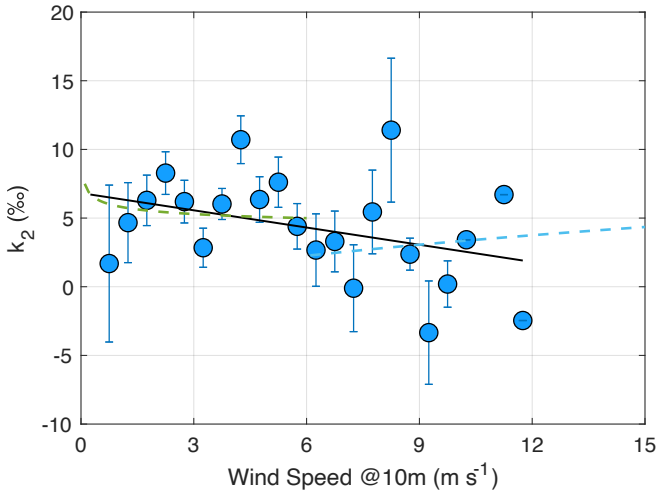

Figure S5: Mean k_2 values obtained for each wind speed class. Dashed lines represent the non-equilibrium fractionation factor parametrization as a function of WS at 10m height. Solid black line represents a linear fit $k_2 = (-0.4 \pm 0.3) * WS + (7 \pm 2)$ ‰ (R^2=0.12) in the wind speed interval 0 – 10 m s^{-1}.

References

Benetti, M., Lacour, J. L., Sveinbjörnsdóttir, A. E., Aloisi, G., Reverdin, G., Risi, C., et al. (2018). A Framework to Study Mixing Processes in the Marine Boundary Layer Using Water Vapor Isotope Measurements. *Geophysical Research Letters*, *45*(5), 2524–2532. https://doi.org/10.1002/2018GL077167

Benetti, Marion, Reverdin, G., Pierre, C., Merlivat, L., Risi, C., Steen-larsen, H. C., & Vimeux, F. (2014). Deuterium excess in marine water vapor: Dependency on relative humidity and surface wind speed during evaporation, 584–593. https://doi.org/10.1002/2013JD020535.Received

Benetti, Marion, Reverdin, G., Aloisi, G., & Sveinbjörnsdóttir, Á. (2017). Stable isotopes in surface waters of the A tlantic O cean: Indicators of ocean-atmosphere water fluxes and oceanic mixing processes. *Journal of Geophysical Research: Oceans*, *122*(6), 4723–4742.

BIOS. (2021). Bermuda Atlantic Time-series Study (BATS).

Brutsaert, W. (1965). A model for evaporation as a molecular diffusion process into a turbulent atmosphere. *Journal of Geophysical Research*, *70*(20), 5017–5024. https://doi.org/10.1029/jz070i020p05017

Geernaert, G. L. (2003). Boundary Layers | Surface Layer. *Encyclopedia of Atmospheric Sciences*, (1988), 305–311. https://doi.org/10.1016/b0-12-227090-8/00092-0

LeGrande, A. N., & Schmidt, G. A. (2006). Global gridded data set of the oxygen isotopic composition in seawater. *Geophysical Research Letters*, *33*(12), 1–5. https://doi.org/10.1029/2006GL026011

Madsen, M. V., Steen-Larsen, H. C., Hörhold, M., Box, J., Berben, S. M. P., Capron, E., et al. (2019). Evidence of Isotopic Fractionation During Vapor Exchange Between the Atmosphere and the Snow Surface in Greenland. *Journal of Geophysical Research: Atmospheres*, *124*(6), 2932–2945. https://doi.org/10.1029/2018JD029619

Merlivat, L. (1978). The dependence of bulk evaporation coefficients on air-water interfacial conditions as determined by the isotopic method. *Journal of Geophysical Research: Oceans*, *83*(C6), 2977–2980.

Merlivat, L., & Jouzel, J. (1979). Global climatic interpretation of the deuterium-oxygen 18 relationship for precipitation. *Ournal of Geophysical Research: Oceans*, *84*(C8), 5029–5033.

Steen-Larsen, H. C., Sveinbjörnsdottir, A. E., Jonsson, T., Ritter, F., Bonne, J. -L., Masson-Delmotte, V., et al. (2015). Moisture sources and synoptic to seasonal variability of North Atlantic water vapor isotopic composition. *Journal of Geophysical Research Atmospheres*, *120*. https://doi.org/10.1002/2015JD023234